ACS OMEGA

Open Access

http://pubs.acs.org/journal/acsodf

Article

Hierarchical Porous Reduced Graphene Oxide/Poly(L-lactic acid) Fiber Films: The Influence of Recrystallization on Strength

Jun Song, Yilu Chen, and Zhongda Chen*

Cite This: *ACS Omega* 2024, 9, 27358−27368

Read Online

ACCESS | Metrics & More | Article Recommendations | Supporting Information

ABSTRACT: Electrospinning technology for fabricating nanofiber films and the Hummer method for synthesizing graphene oxide (GO), along with subsequent reduction, have been significantly advanced, demonstrating immense potential for large-scale industrial applications. Nanofibrous films loaded with reduced graphene oxide (rGO) have been widely explored for their applications in electromagnetic shielding, the biomedical fields, and pollutant adsorption. However, fragile mechanical performance of electrospun fibers with limited surface post-treatment methods has somewhat hindered their further industrial development. In response to this challenge, we propose a dual-regulation strategy involving post-treatment to form porous nanofiber films and the controlled flake size of rGO for surface coating during preparation. This approach aims to achieve poly(L-lactic acid) (PLLA)/rGO electrospun fibrous films with enhanced mechanical properties. It offers a roadmap for the continued application and standardized production of fibrous films loaded with rGO.

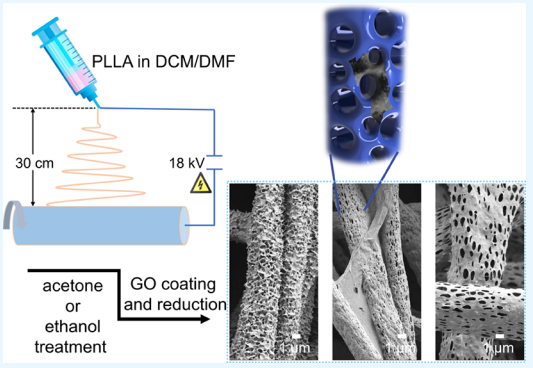

1. INTRODUCTION

Polyester materials, as a category of engineering plastics with excellent mechanical performances, have a wide range of uses.[1] Among them, 80% of polyester is processed into fibers. With the establishment of the United Nations Sustainable Development Goals, choosing biodegradable polyesters to replace the widely used polyethylene terephthalate (PET), polybutylene terephthalate, and so forth, has significant environmental value.[2] Among biodegradable polyester polymers, poly(L-lactic acid) (PLLA) has attracted widespread attention.[3]

Electrospinning, a technique for fabricating polymer nanofibers with the potential for large-scale production, has been extensively researched in the academic and partly industrialized areas. Specifically concerning PLLA, the electrospinning process involves ejecting a PLLA spinning solution, dissolved in dichloromethane (DCM), into the air, followed by solvent evaporation.[4] The addition of a nonsolvent for PLLA, such as *N*,*N*-dimethylformamide (DMF), results in the uniform distribution in the DCM/DMF/PLLA liquid phase solution.[5] During the fiber formation process, the evaporation rate of DMF is significantly slower than that of DCM, and DMF occupies some area in the PLLA fibrous structure, leading to the formation of pores on both the surface and interior of fibers.[6] With micrometer-scaled pores present among the fibers, the resulting electrospun fibrous film exhibits hierarchical porosity (micropores among fibers and nanoscaled pores on the fibers' surface and interior).[7] Subsequently, during post-treatment, PLLA undergoes recrystallization via physical or chemical methods, effectively altering the morphology of the mesopores within the fibers. Previous studies have shown that immersing PLLA or polyethylene terephthalate (PET) porous fibers in acetone or ethanol further modifies the mesopore morphology.[8,9]

The hierarchical porous structure offers numerous benefits, including a high specific surface area and potential for functional loading.[10] This structure holds significant promise for applications in various fields such as biology,[11] energy,[12] and environmental protection.[13] However, the practical use of PLLA electrospun fibrous material is often constrained due to PLLA's hydrophobic nature, leading to poor cell adhesion and weak mechanical strength of the PLLA electrospun film.[14,15]

Graphene is a single-layer two-dimensional (2D) crystal composed of carbon atoms arranged in the sp^2 hybrid orbital according to a honeycomb crystal lattice. Graphene has many excellent properties such as high mechanical strength, light transmittance, thermal conductivity, carrier mobility, and specific surface area.[16] Consequently, graphene is often employed to optimize the physical or chemical properties of polymer matrices. Additionally, graphene oxide (GO), one of the most used graphene derivatives, exhibits good hydro-

Received: February 29, 2024
Revised: May 31, 2024
Accepted: June 4, 2024
Published: June 12, 2024

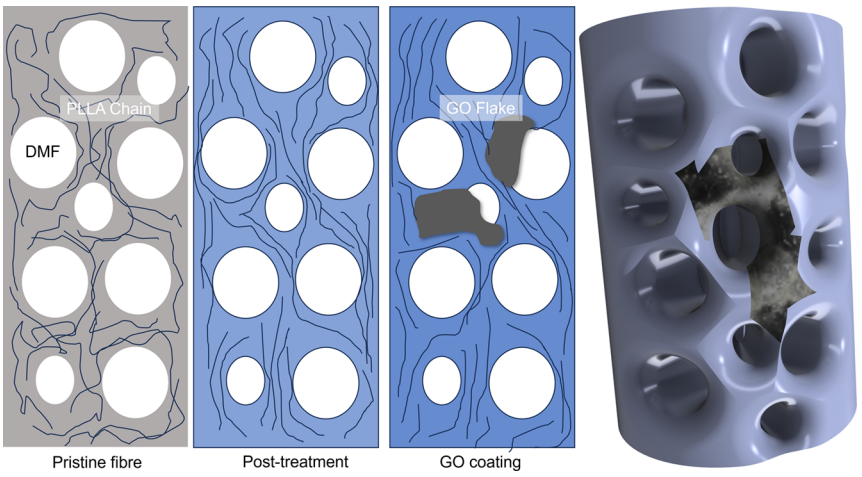

Figure 1. Schematic diagram of the electrospun PLLA/rGO fiber-forming processes.

philicity and easy dispersibility in water.[17] The oxygen-containing functional groups of GO can strongly interact with the composite matrices, forming a robust bonding interface, thereby improving the material performances.[17]

Here, we regulated the composition of spinning solutions and employed various post-treatment methods to compare a range of PLLA/rGO fibers with different hierarchical porous structures, as Figure 1 demonstrates. During the post-treatment process, the recrystallization of PLLA occurs through physical or chemical methods, effectively altering the morphology of mesopores within the fibers. Additionally, in our experiments, immersing PLLA porous fibers in acetone or ethanol further modifies the morphology of mesopores.

The fiber' surface treated with ethanol exhibits a relatively smooth texture, attributed to the longer length of PLLA molecular chains compared to those treated with acetone. This smoother surface provides favorable conditions for the subsequent loading and reduction of GO. The uniform coating of graphene oxide is achieved by mixing ethanol-soaked PLLA fiber films with a graphene oxide aqueous solution by using ultrasonication. Subsequently, GO on the fibers undergoes reduction through prolonged immersion in a relatively high-temperature L-(+)-ascorbic acid (LAA) solution to PLLA/rGO fibrous films. In both steps, ultrasonication and high temperature are typical physical means of inducing PLLA recrystallization.

2. MATERIALS AND METHODS

2.1. Materials. PLLA (PL-65) pellets were supplied by PURAC Biochem B.V., The Netherlands. DCM (≥99.9%, Sigma-Aldrich) and DMF (≥99.8%, Sigma-Aldrich) were used to prepare electrospinning solutions. Ethanol (≥99.8%, VWR Chemicals) and acetone (≥99.8%, Fisher Chemical) were used for the post-treatment of the electrospun films. Expandable graphite flakes were purchased from Sigma-Aldrich Company Ltd., with a particle size of over 300 μm. Sulfuric acid (≥95%, Fisher Chemical), potassium permanganate (≥99.0%, Alfa Aesar), 30% (w/v) hydrogen peroxide (Fisher Chemical), and 37% hydrochloric acid (Fisher Chemical) were used for GO synthesis. L-(+)-Ascorbic acid (LAA) (99%, Sigma-Aldrich) was used to reduce GO to rGO.

2.2. Fabrication of PLLA Electrospun Films. PLLA pellets were dried at 50 °C for 2 h and then added to DCM at a certain weight ratio range from 1.4 to 2.2 wt %. The PLLA/DCM solution was heated and stirred at 50 °C for 1.5 h. After the solution was cooled to room temperature, DCM that evaporated during the heating process was added up into the solution, and DMF with a certain weight ratio was subsequently added. The concentrations of PLLA were set as 2.2, 2.0, 1.8, 1.6, and 1.4 wt % for comparison. DMF was fixed at 5% of solution when regulating the concentrations of PLLA. The concentrations of DMF in the solution were set as 10, 7.5, 5, 2.5, and 0 wt % for comparison. The concentrations of PLLA were fixed at 2.0 wt % when regulating the ratio of DMF in the solution.

An electrospinning setup (TONGLI TECH TL-Pro, China) equipped with a syringe pump was used to fabricate the electrospun films. The solution was fed at a constant flow rate of 6 mL/h by the pump. The drum was rotated at 60 rpm. A high voltage of +15 kV and a low voltage of −3 kV were, respectively, applied to the needle and the collector. The distance between the needle and collector was fixed at 30 cm.

For acetone and ethanol treatment, the electrospun PLLA films immersed in acetone for 5 min were marked as DCM-acetone, while films immersed in ethanol for 5 min were marked as DCM-ethanol or non-DCM.

2.3. Preparation of GO and PLLA/rGO Films. 1.5 g of expandable graphite placed in a beaker was heated in a microwave (Frigidaire, UK) at 700 W for 30 s. Then, the expanded graphite was transferred to a 2 L three-neck round-bottom flask which was put in a water bath. Sulfuric acid (300 mL) and 15 g of potassium permanganate were subsequently slowly added in the flask, and the flask was sealed and stirred by an overhead stirrer for 24 h. The water bath was first changed to ice water bath, and 300 mL of DI water and 50 mL of hydrogen peroxide were then slowly added into the flask. After 30 min, 300 mL of 10% diluted hydrochloric acid was finally added in. The GO suspension was washed 10 times to neutral by a centrifuge with DI water.

A portion of 5 mL of water-based GO suspension was first ultrasound at 75 W for 4 h and centrifuged at 10,000 rpm for 60 min. The upper layer suspension was kept in order to obtain a relatively small amount of graphene oxide (SGO). The other water-based GO suspension was directly centrifuged at 10,000 rpm for 20 min. The lower layer suspension was kept in order to obtain large graphene oxide (LGO), a GO with relatively large particle size.

https://doi.org/10.1021/acsomega.4c01976
ACS Omega 2024, 9, 27358−27368

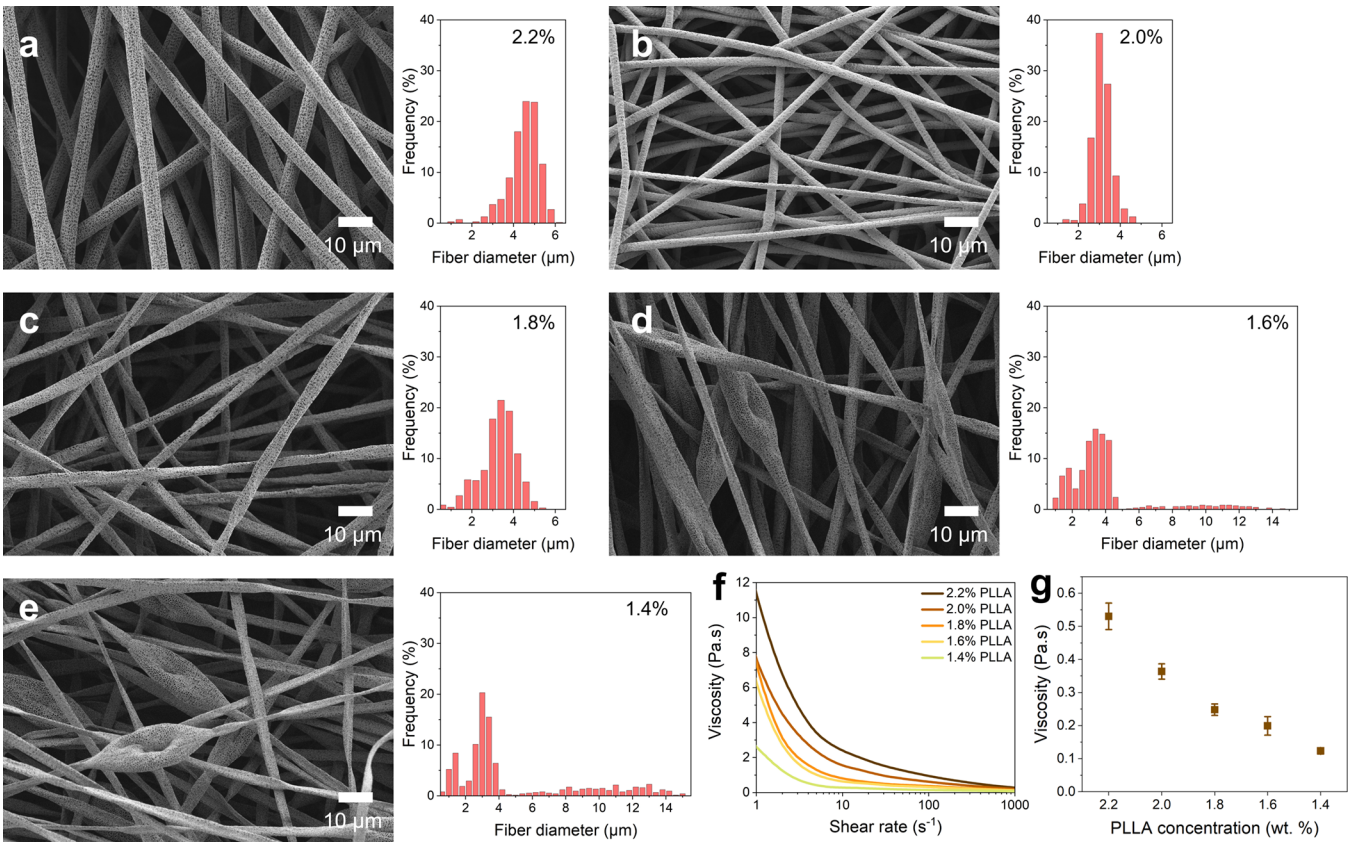

Figure 2. SEM images and diameter distribution histograms of the electrospun fibers obtained from the 5.0 wt % DMF electrospinning solutions with different PLLA concentrations: (a) 2.2 wt %, (b) 2.0 wt %, (c) 1.8 wt %, (d) 1.6 wt %, and (e) 1.4 wt %. (f) Relationship between the shear viscosity and shear rate of the 5.0 wt % DMF electrospinning solutions with different PLLA concentrations. (g) Relationship between the shear viscosity and PLLA concentration of the 5.0 wt % DMF electrospinning solutions at the shear rate of 326.54 s^{-1}.

The PLLA fibrous films for GO coating were first ultrasound in 5 mL of water-based GO suspensions (3 mg/mL) at 75 W for 30 min and dried at room temperature for 24 h in order to obtain composite films of PLLA and GO. Some of the PLLA/GO electrospun films were subsequently immersed in 5 mg/mL LAA aqueous solution for 48 h, rinsed in DI water, and dried at room temperature for 24 h to obtain composite films of PLLA/rGO. Similar to the classification of GO flake size, the electrospun PLLA fibrous film-coated LGO and reduced was marked as PLLA/LrGO films, while the film-coated SGO and reduced was marked as PLLA/SrGO films.

2.4. Characterization. Prior to viscosity measurement, the electrospinning solutions were mixed on a hot plate stirrer (Stuart SB 162-3, UK) at level 2 for 5 min. A Discovery Hybrid Rheometer (TA Instruments HR-3, USA) equipped with a 60 mm stainless steel Peltier parallel-plate geometry was employed to study the viscosity of the electrospinning solutions. Hence, the shear rate was set at 326.54 s^{-1} to carry out the test. All of the tests were performed at 25 °C with a test gap of 1000 μm.

The field emission gun scanning electron microscopy (FEGSEM) instrument (Zeiss Ultra 55, Germany) was used to take SEM images, and the operating voltage was 1.5 kV. An FTIR spectrometer (Thermo Nicolet 5700, USA) using OMINC software equipped with Far IR option and Smart Orbit Diamond ATR accessory was, respectively, used to collect the FTIR spectra of circular pellet samples of GO or rGO and square samples of PLLA electrospun films. An X-ray diffractometer (PANalytical X'Pert Pro, USA) equipped with a copper-sealed tube target was used to collect XRD patterns. A Raman spectrometer (Renishaw System 1000, UK) equipped with a 50x objective and a 514 nm diode laser was used to record the Raman spectra of the electrospun samples. The film was cut into square samples with a side length of 1 cm and fixed on a glass slide with the aid of a double-sided tape. An optical contact angle meter system (Krüss DSA100, Germany) was used to measure the water contact angle. X-ray photoelectron spectroscopy (XPS) was performed with Kratos Axis (Kratos Analytical Limited, Japan), using monochromatized Al Kα radiation.

An atomic force microscopy (AFM) instrument (Park NX20) was used to check the surface morphology of rGO both on the silicon wafer and on the surface of the PLLA fiber (DMF-ethanol). Samples were measured by a noncontact probe (PPP-NCHR, force constant = 42 N/m).

2.5. Mechanical Performances. The tensile test sample was prepared with the effective area of the sample being a 25 mm × 5 mm rectangle. A digital thickness gauge (RS Pro, UK) was used to measure the thickness of each sample, and tensile testing was carried out by using a static testing machine (Instron 3344, USA) equipped with a 5 N cell load. The stretching speed was set at 5 mm/min. At least five samples of each film were tested for the mechanical properties of the film.

The results of mechanical performances were presented as mean ± standard deviation.

https://doi.org/10.1021/acsomega.4c01976
ACS Omega 2024, 9, 27358−27368

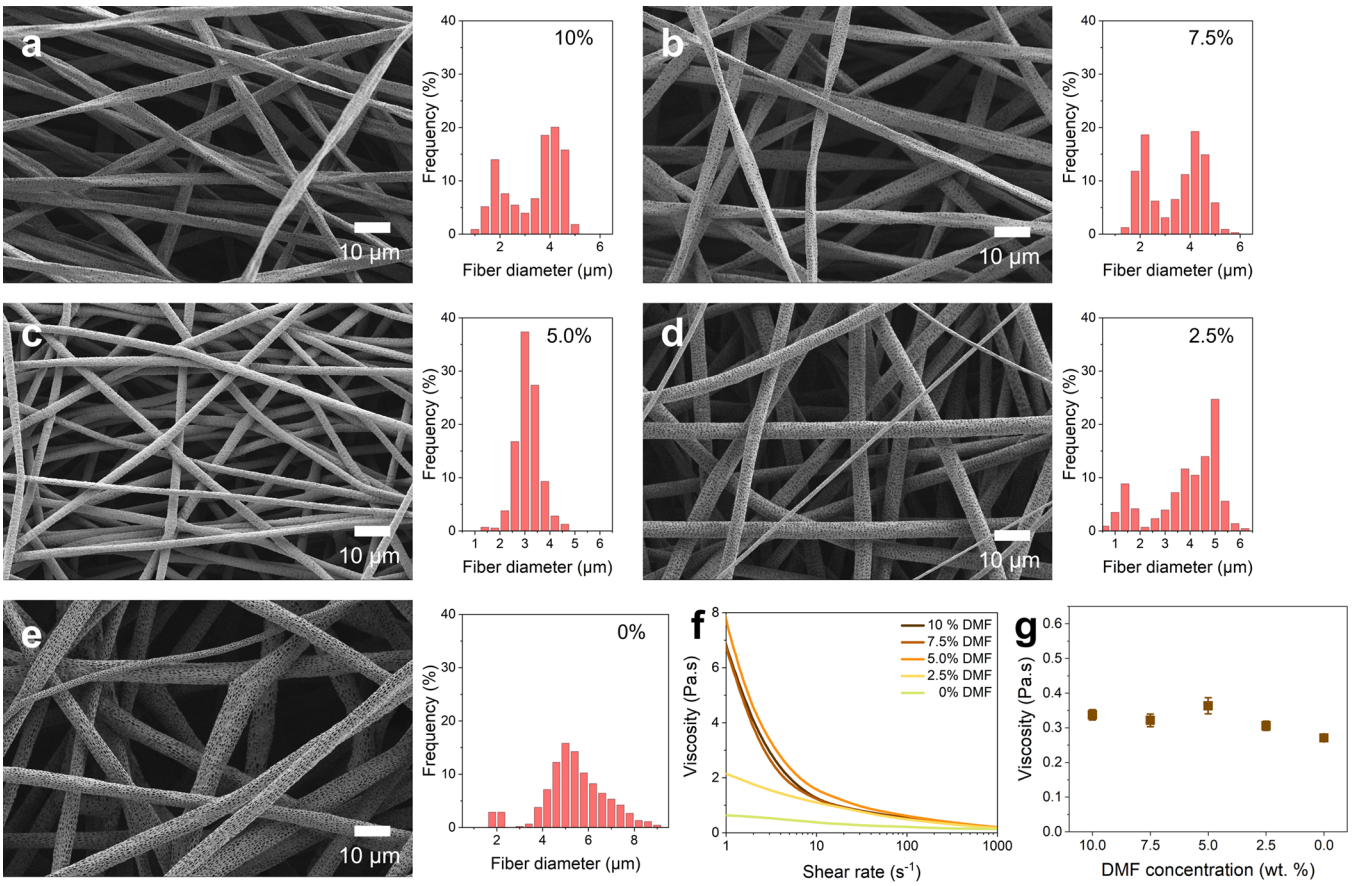

Figure 3. SEM images and diameter distribution histograms of the electrospun fibers obtained from the 2.0 wt % PLLA electrospinning solutions with different DMF concentrations: (a) 10.0 wt %, (b) 7.5 wt %, (c) 5.0 wt %, (d) 2.5 wt %, and (e) 0.0 wt %. (f) Relationship between the shear viscosity and shear rate of the 2.0 wt % PLLA. (g) Relationship between the shear viscosity and DMF concentration of the 2.0 wt % PLLA electrospinning solutions at the shear rate of 326.54 s^{-1}.

3. RESULTS AND DISCUSSION

3.1. Effect of PLLA Concentration on Electrospun Fiber Diameter. Figure 2 presents the surface morphology of electrospun fibers with different concentrations of PLLA in the DCM/DMF solution. The obtained electrospun fibers had a uniform thickness when the PLLA concentration of electrospinning solution reached 2.0 wt %. Besides, the lower the PLLA concentration was, the finer the fiber became and the narrower the fiber diameter distribution was. When the PLLA concentration was reduced from 2.2 to 2.0 wt %, the fiber diameter was reduced from 4.5 ± 0.7 μm (Figure 2a) to 3.1 ± 0.5 μm (Figure 2b). When the PLLA concentration was decreased to 1.8 wt %, the thickness of the obtained electrospun fibers became uneven significantly. In Figure 2c, the thicker region of the fiber was 3.6 ± 0.6 μm, and the thinner region was only 1.8 ± 0.4 μm. Compared with the electrospun fibers from 2.0 and 2.2 wt % spinning solutions, those of fibers from 1.8 wt % spinning solution appeared flat, and the fiber diameter distribution was also widened. When the PLLA concentration was as low as 1.6 wt %, beads were formed. The maximum diameter of the beads was 9.8 ± 2.2 μm. Besides, the fibers were flatter, and with the PLLA concentration further reduced, the beads became shorter and fatter, and the fibers became flatter and finer.

In Figure 2f,g, it is observed that the shear viscosity of the 5.0 wt % DMF electrospinning solutions decreased as the shear rate increased, indicating that these solutions were shear-thinning fluids. Regardless of the influence of the various interfaces through which the electrospinning solution passed during the electrospinning process on the flow rate of the electrospinning solution, the flow rate of 6 mL/h in this work corresponded to the shear rate of 326.54 s^{-1}. The shear viscosity of the electrospinning solution at this shear rate increased as the PLLA concentration increased. This conclusion is consistent with the study by Wojasiński et al.[18]

3.2. Effect of DMF Concentration on the Electrospun Fiber Diameter. Figure 3 presents the surface morphology of the obtained electrospun fiber from the 2.0 wt % PLLA electrospinning solutions with varying DMF concentrations. It could be found that the fibers from the spinning solution with 5.0 wt % DMF concentration had a relatively uniform thickness and a relatively small fiber diameter. When the DMF concentration was lower than 5.0 wt %, the diameter of the electrospun fibers increased with the decrease of the concentration of DMF. Specifically, the fiber diameter of the non-DMF group was 1.74 times that of the fibers spun from 5 wt % DMF solutions. Besides, for one single electrospun fiber of 2% PLLA without DMF, the thickness of the fiber was still uniform, while the difference in fiber diameter between fibers became large, which results in a wide fiber diameter distribution. Moreover, when the DMF concentration exceeded 5.0 wt %, the fiber diameter stabilized at around 3.0 μm, with the electrospun fibers becoming flatter. Hence, the wider fiber diameter distribution of these fibers was mainly

https://doi.org/10.1021/acsomega.4c01976
ACS Omega 2024, 9, 27358−27368

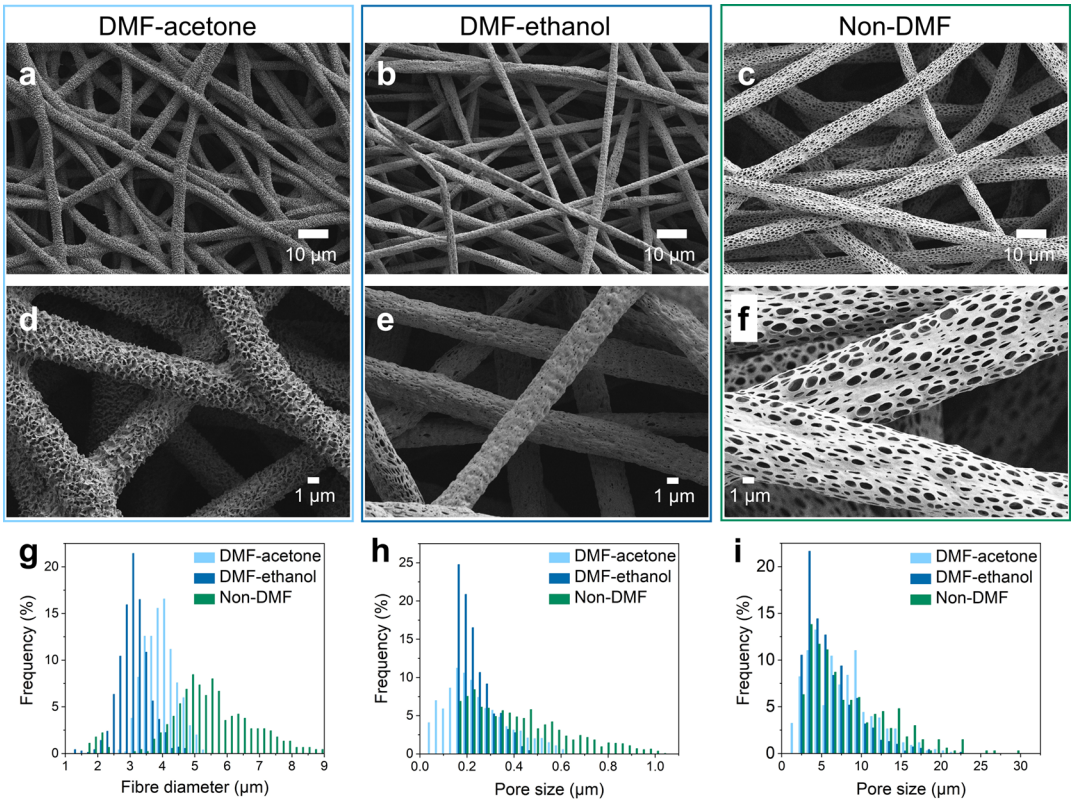

Figure 4. Surface morphology and parameters of electrospun PLLA fibers. (a, d) Surface morphology of electrospun PLLA fibers dissolved by the DCM/DMF dual-solvent and post-treated by acetone (DMF-acetone). (b, e) Surface morphology of electrospun PLLA fibers dissolved by the DCM/DMF dual-solvent with ethanol treatment (DMF-ethanol). (c, f) Surface morphology of electrospun PLLA fibers dissolved by only DCM solvent without any treatment (non-DMF). (g) Fiber diameter distribution histograms of the three kinds of electrospun PLLA mentioned above. (h) Size distribution histograms of the pores on the surface of the fiber. (i) Size distribution histograms of the pores among the fibers.

caused by the difference in fiber diameter on an individual fiber rather than the difference in fiber diameter between fibers. Based on the analysis provided, 2% PLLA with DMF 5 wt % in the solution film had the finest diameter and the most uniform thickness.

As can be seen from Figure 3f,g, the shear viscosity of the 2.0 wt % PLLA electrospinning solutions decreased as the shear rate increased, indicating that these solutions also exhibited a shear-thinning behavior. The shear viscosity of an electrospinning solution containing non-DMF was relatively less affected by the shear rate than the other DMF-containing electrospinning solutions. The shear viscosities of the electrospinning solutions at a shear rate of 326.54 s^{-1} were similar.

3.3. Surface Morphology of PLLA Fibers with Different Post-Treatments. As can be seen from Figure 4, the surface morphology of the electrospun fibers varied among the DMF-acetone, DMF-ethanol, and non-DMF films. Among them, the DMF-ethanol fiber obtained from the 2.0 wt % PLLA electrospinning solution with a DMF concentration of 5.0 wt % exhibited the finest and owned the smoothest surface. In contrast, the non-DMF fiber, fabricated from the 2.0 wt % PLLA electrospinning solution without adding DMF was much thicker and featured many visible pores on its surface. These changes in the non-DMF film compared to the DMF-ethanol film showed the electrospinning solution without DMF volatilized faster, and the PLLA molecular chains did not have enough time to stretch and form, so these electrospun fibers are thick and porous.[6]

Naga et al. conducted a study on the crystallization of amorphous PLLA induced by organic solvents.[19] Among the various organic solvents investigated in their research, acetone is the most effective solvent for promoting the crystallization of amorphous PLLA. PLLA crystallized into α crystals. Additionally, acetone also acted as a plasticizer. As acetone volatilized, PLLA films experienced a transition from being soft and ductile to hard and brittle. The surface of the DMF-acetone fiber exhibited significant roughness, and the originally smooth fiber formed a very large number of open pores on the surface, which made the fiber of the DMF-acetone film look like a bare corncob. Besides, the DMF-acetone fiber was slightly thicker than the DMF-ethanol fiber.The pristine PLLA fibers spun with DMF were originally independent. After post-treated only with acetone, the pristine PLLA fibers spun with DMF formed a whole at the intersection with each other. These changes in the DMF-acetone film compared to the DMF-ethanol film were caused by the acetone post-treatment that induces recrystallization and a slight dissolve of the PLLA molecular chains of the electrospun fibers.[20]

3.4. Surface Morphology of PLLA Fibers Coated with GO Nanosheets. Currently, both the electrospinning technology for the fabrication of nanofiber films and the Hummer method for the synthesis of rGO[21] have matured considerably, exhibiting great potential for large-scale industrial applications. Nanofibrous films loaded with reduced graphene oxide have been extensively reported for their applications in biology,[11] energy,[12] and environmental protection.[13] This approach aims to achieve a PLLA/graphene electrospun

https://doi.org/10.1021/acsomega.4c01976
ACS Omega 2024, 9, 27358−27368

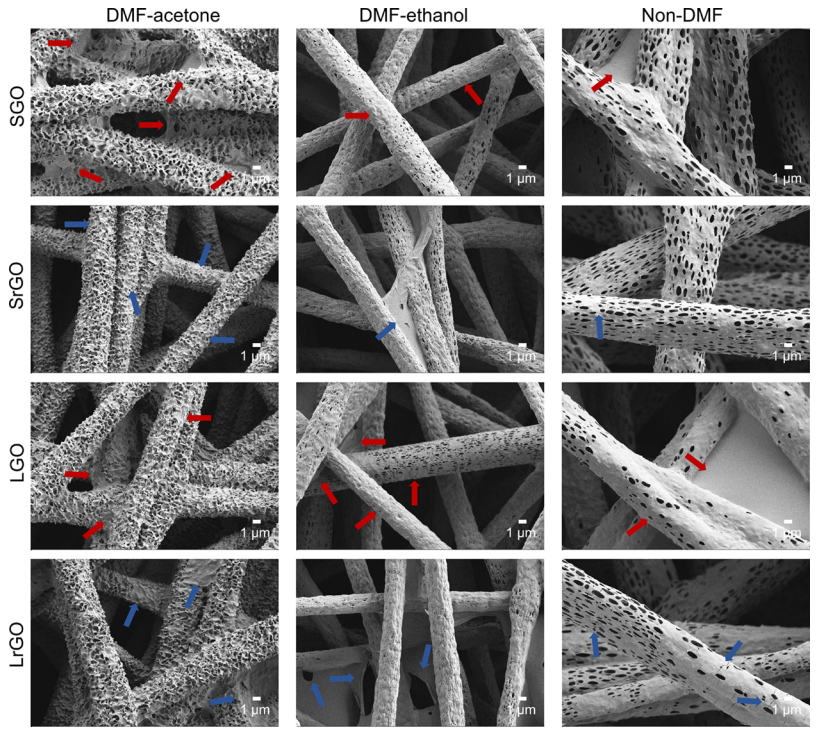

Figure 5. SEM images of GO- and rGO-coated DMF-acetone, DMF-ethanol, and non-DMF films with a magnification of 2.5 K. Scale bars: 1 μm.

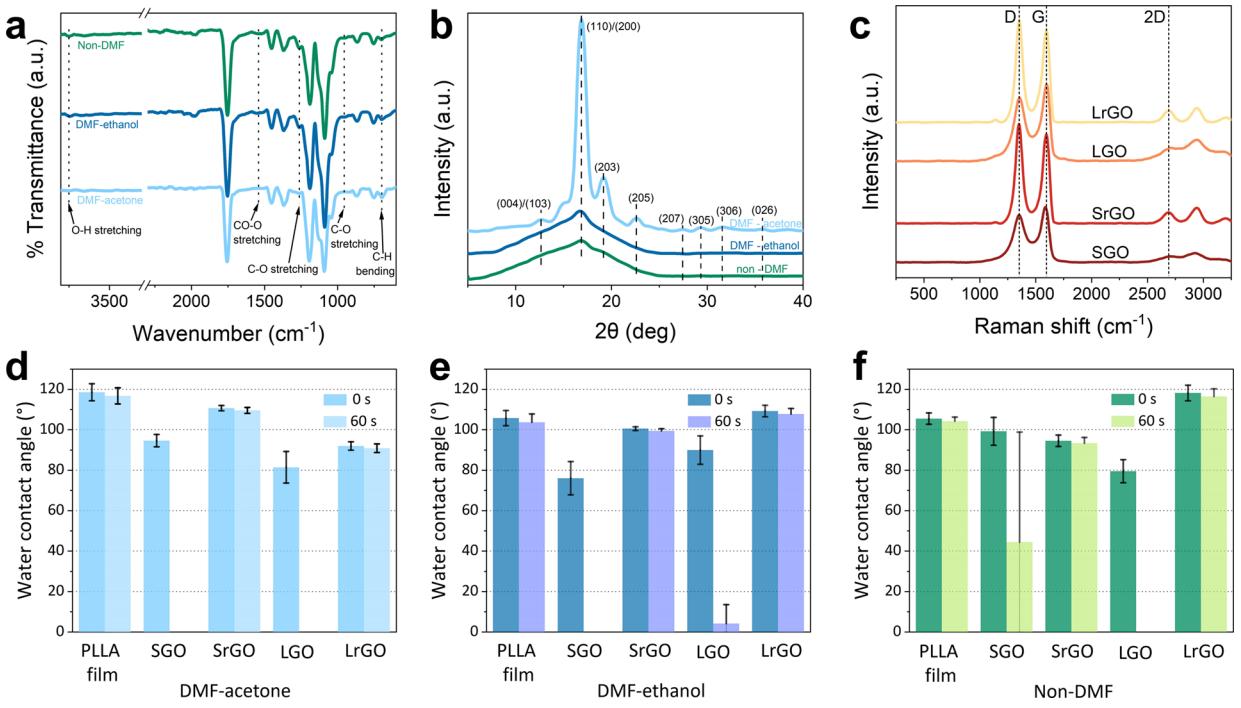

Figure 6. Material characterizations of three kinds of PLLA/rGO films. (a) FT-IR spectra of DMF-acetone, DMF-ethanol, and non-DMF PLLA films. (b) XRD patterns of DMF-acetone, DMF-ethanol, and non-DMF PLLA films. (c) Raman spectra of SGO, SrGO, LGO, and LrGO nanosheets. (d) Water contact angle of the DMF-acetone group PLLA film with rGO coating. (e) Water contact angle of the DMF-ethanol group PLLA film with rGO coating. (f) Water contact angle of the non-DMF group PLLA film with rGO coating.

composite with enhanced mechanical properties. It provides guidance for further industrial application and standardized production of fiber films loaded with rGO.

The fiber diameter of the DMF-ethanol film was 3.12 ± 0.48 μm, whereas the fiber diameter of the DMF-acetone film, which was post-treated by acetone, was increased to 3.97 ± 0.49 μm. The fiber diameter of the non-DMF film prepared by the electrospinning solution without DMF was more than 1.5 times the fiber diameter of the DMF-ethanol film obtained from the electrospinning solution with DMF and was 5.38 ± 1.38 μm. Ideally, all SGO could be coated onto the fiber surface of the above three reference films, but a significant

https://doi.org/10.1021/acsomega.4c01976
ACS Omega 2024, 9, 27358−27368

portion of LGO flake size was larger than the fiber diameters, and this kind of LGO could cover one or more electrospun fibers. The pore sizes of the electrospun fibers obtained from the DMF-acetone, DMF-ethanol, and non-DMF films were 0.24 ± 0.13, 0.24 ± 0.07, and 0.42 ± 0.20 μm, respectively. Combining the flake size of SGO and LGO, it is known that in most cases the pores on the electrospun fibers of the DMF-acetone and DMF-ethanol films could be completely covered by SGO or LGO, and because the pores on the electrospun fibers of the DMF-acetone and DMF-ethanol films were relatively small, the SGO or LGO even with a small flake size was difficult to enter. Some pores of the non-DMF electrospun fibers might be covered by LGO with a large flake size, while the others might hold a certain amount of SGO or LGO with a small flake size. The interfiber pore sizes of the DMF-acetone, DMF-ethanol, and non-DMF films were similar, being 7.39 ± 3.92, 6.17 ± 3.25, and 8.46 ± 5.13 μm, respectively.

It can also be seen from Figure 5 that the regions where the interfiber pore sizes are mainly distributed coincide with each other with a high probability. When considering the flake sizes of small graphene oxide (SGO) and large graphene oxide (LGO), it becomes apparent that the majority of SGO and LGO particles could move freely between interfiber pores. Only a small amount of LGO with a large flake size might cover the interfiber pores of the electrospun film.

3.5. Material Characterizations of PLLA Fibers Coated with GO Nanosheets. Figures 6a and S10−S12 show the FTIR spectra of DMF-acetone, DMF-ethanol, and non-DMF electrospun films. It can be seen from the figure that the PLLA electrospinning film post-treated by acetone rarely possesses the absorption bands due to the O−H stretching vibration (at ∼3750 cm^{-1}) and CO-O stretching vibration (from 1587 to 1485 cm^{-1}) in the carboxylic acid group.[22] This film does not have the absorption bands because of the C−O stretching vibration (at 1261 and ∼955 cm^{-1}) in the alcoholic hydroxyl group neither. This reveals that the porous post-treatment by acetone largely eliminated the hydroxyl groups at both ends of the PLLA molecular chain. Thus, the C−H bending vibration at 698 cm^{-1} of the DMF-acetone film is stronger than that of the DMF-ethanol and non-DMF films.[23]

Figures 6b and S7−S9 show the XRD patterns of DMF-acetone, DMF-ethanol, and non-DMF PLLA films. These patterns exhibit a distinct diffraction peak at 2θ = 16.86°, 16.72°, and 16.82°, respectively. This peak corresponds to the (110)/(200) planes as Tables S3 and S4 presented. Furthermore, the DMF-ethanol and non-DMF films display no additional diffraction peaks apart from this diffraction peak which is relatively broader and weaker. In contrast, the XRD pattern of the DMF-acetone film reveals narrower and stronger diffraction peaks in addition to the main peak. This illustrates the disordered structure of the DMF-ethanol and non-DMF films and the ordering structure of the DMF-acetone film. Essentially, the DMF-ethanol and non-DMF films were amorphous, while the DMF-acetone film exhibits crystalline characteristics.[24] This enhancement in crystallinity is attributed to the post-treatment with acetone, which effectively improves the crystallinity of the PLLA electrospun film. At the diffraction peak corresponding to the (110)/(200) planes, the full width at half-maximum (fwhm) of DMF-ethanol which is 6.59 is smaller than that of non-DMF which is 8.41. This indicates that the crystallinity of the DMF-ethanol film is higher than that of the non-DMF film.[25] This difference may be because DMF was added to the electrospinning solution used to fabricate the DMF-ethanol film, which delayed the volatilization of the electrospinning solution and gave the PLLA molecular chains more time to align orderly. However, DMF was not added to the electrospinning solution used to fabricate the non-DMF film, resulting in a relatively rapid volatilization of the solution and insufficient time for orderly alignment of PLLA molecular chains before the film structure was set. Hence, the DMF-acetone film was in α-form crystal while the DMF-ethanol and non-DMF films were in α''-form crystal.[24]

Figures 6c and S4−S6 display the Raman spectra of SGO, SrGO, LGO, and LrGO. All these four samples have three dominant peaks, D, G, and 2D peaks. The D peaks of SGO, SrGO, LGO, and LrGO are at positions of 1352, 1351, 1355, and 1352 cm^{-1}, respectively. This peak is associated with a breathing mode of j-point photons of A1g symmetry[26] and is attributed to the presence of the C=C double bond. The G peaks of SGO, SrGO, LGO, and LrGO are observed at the positions of 1587, 1595, 1597, and 1595 cm^{-1}, respectively. These peaks are associated with the first-order scattering of E2g phonons by sp^2 carbon and attributed to the presence of the stretching C−C single bond, which is caused by the destruction of the C=C double bond. In other words, these peaks are attributed to the sp^3 defect in the sp^2 lattice.[27] The 2D peaks of SGO, SrGO, LGO, and LrGO are at positions of 2709, 2687, 2709, and 2693 cm^{-1}, respectively. These peaks are associated with two phonons with opposite wave vectors that satisfy the motion conservation process and can be activated without defects in graphene.[28] The findings from the Raman spectra are further supported by the SEM images presented in Parts S1 and S2. The SEM images in Figures S1 and S2 also prove these results.

Figure 6d−f presents the water contact angle test result that determines the hydrophilicity and hydrophobicity of the PLLA electrospun films. Both the DMF-acetone/SGO and DMF-acetone/LGO films exhibit superhydrophilicity, while the DMF-acetone/SrGO and DMF-acetone/LrGO films are hydrophobic. When the droplet just landed on the film, the water contact angles recorded on the DMF-acetone/SGO and DMF-acetone/LGO films are 95 ± 3° and 81 ± 8°, respectively. Also, the DMF-acetone/LGO film absorbed the droplet landed on its surface faster than the DMF-acetone/SGO film. This reveals that the DMF-acetone film coated with GO of a large flake size has a higher moisture absorption rate. The hydrophobicity of the DMF-acetone/SrGO and DMF-acetone/LrGO films obtained by the reduction of LAA aqueous solution was significantly improved but not superior to the original DMF-acetone film. Besides, the hydrophobicity of the DMF-acetone/SrGO film was superior to that of the DMF-acetone/LrGO film. The water contact angles of these two films are increased to 111° and 92°, respectively.

In Figure 6e, both the DMF-ethanol/SGO and DMF-ethanol/LGO films are observed to be superhydrophilic, while the DMF-acetone/SrGO and DMF-acetone/LrGO films are observed to be hydrophobic. However, not every sample of the DMF-ethanol/LGO film completely absorbed water within 60 s of the landing of the droplet on the film. This is due to the uneven distribution of LGO coated on the DMF-ethanol film. At some parts of the DMF-ethanol films, there might not be enough LGO coated by ultrasound. The change in the water contact angle of the DMF-ethanol/SGO and DMF-ethanol/LGO films over time is visible in Figure 6e. When the droplet just landed on the film, the water contact angles recorded on the DMF-ethanol/SGO and DMF-ethanol/LGO films are 76

https://doi.org/10.1021/acsomega.4c01976
ACS Omega 2024, 9, 27358−27368

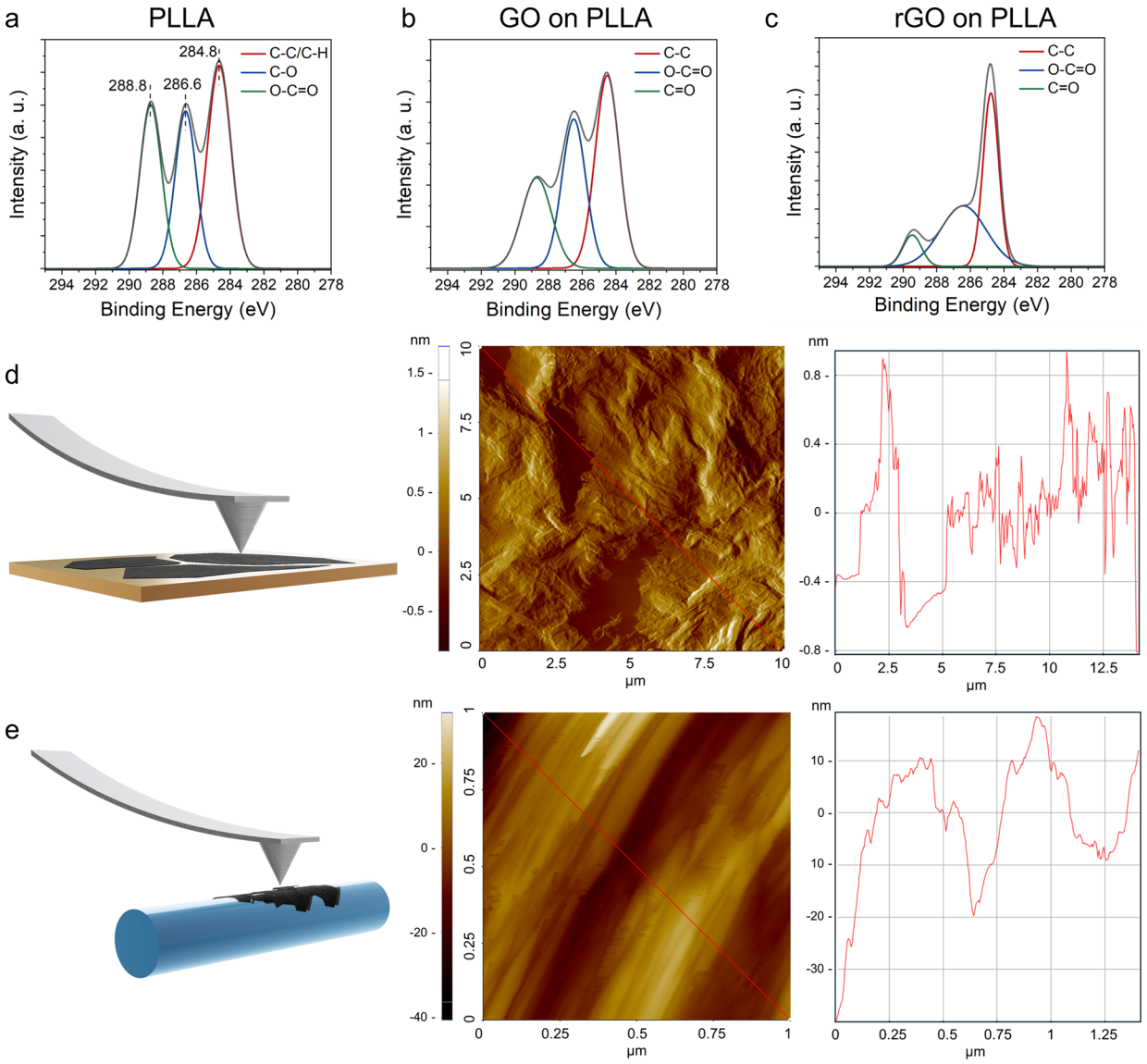

Figure 7. XPS and AFM results of electrospun PLLA fibers. XPS spectrum of (a) electrospun PLLA fibers dissolved by DCM/DMF dual-solvent with ethanol treatment (DMF-ethanol), (b) GO-coated DMF-ethanol electrospun PLLA fibrous films, and (c) rGO-coated DMF-ethanol electrospun PLLA fibrous films. AFM results of (d) rGO on a silicon wafer and (e) rGO on a DMF-ethanol electrospun PLLA fiber.

± 8° and 90 ± 7°, respectively. When the film was coated with enough GO, the moisture absorption rate of the DMF-acetone/LGO film is higher than that of the DMF-ethanol/SGO film. Because some parts of the DMF-ethanol film were not ultrasound with sufficient LGO, the PLLA electrospun fibers were not fully wrapped by LGO and still partially exposed so that these parts could not absorb the droplet entirely and the water contact angle of these parts could not decrease to 0°. The hydrophobicity of the DMF-ethanol/SrGO and DMF-ethanol/LrGO films obtained by the reduction of the LAA aqueous solution was remarkably improved. The hydrophobicity of the DMF-ethanol/LrGO film is even better than that of the pristine DMF-ethanol film. The water contact angles of these two films are increased to 101° and 109°, respectively.

In Figure 6f, the non-DMF/LGO film is superhydrophilic, and the non-DMF/SrGO and non-DMF/LrGO films are hydrophobic. The distribution of SGO coated on the non-DMF film was rather uneven, resulting in some part of the non-DMF/SGO film being superhydrophilic and some part being hydrophobic. When the droplet just landed on the film, the water contact angles recorded on the non-DMF/SGO and non-DMF/LGO films are 99 ± 7° and 80 ± 6°, respectively. When the film was coated with enough GO, the moisture absorption rate of the non-DMF/LGO film is higher than that of the non-DMF/SGO film. However, since SGO distributed on the non-DMF film with the aid of ultrasound was rather uneven, the water contact angle of the film where there was an insufficient amount of SGO could not decrease to 0° and where there was almost no SGO was only reduced by 1° within 60 s of the landing of the droplet on the film. The hydrophobicity of the non-DMF/SrGO and non-DMF/LrGO films obtained after reduction by LAA aqueous solution was significantly improved. The hydrophobicity of the non-DMF/LrGO film is even better than that of the original non-DMF film. The water contact angles of these two films are increased to 85° and 118°, respectively.

https://doi.org/10.1021/acsomega.4c01976
ACS Omega 2024, 9, 27358−27368

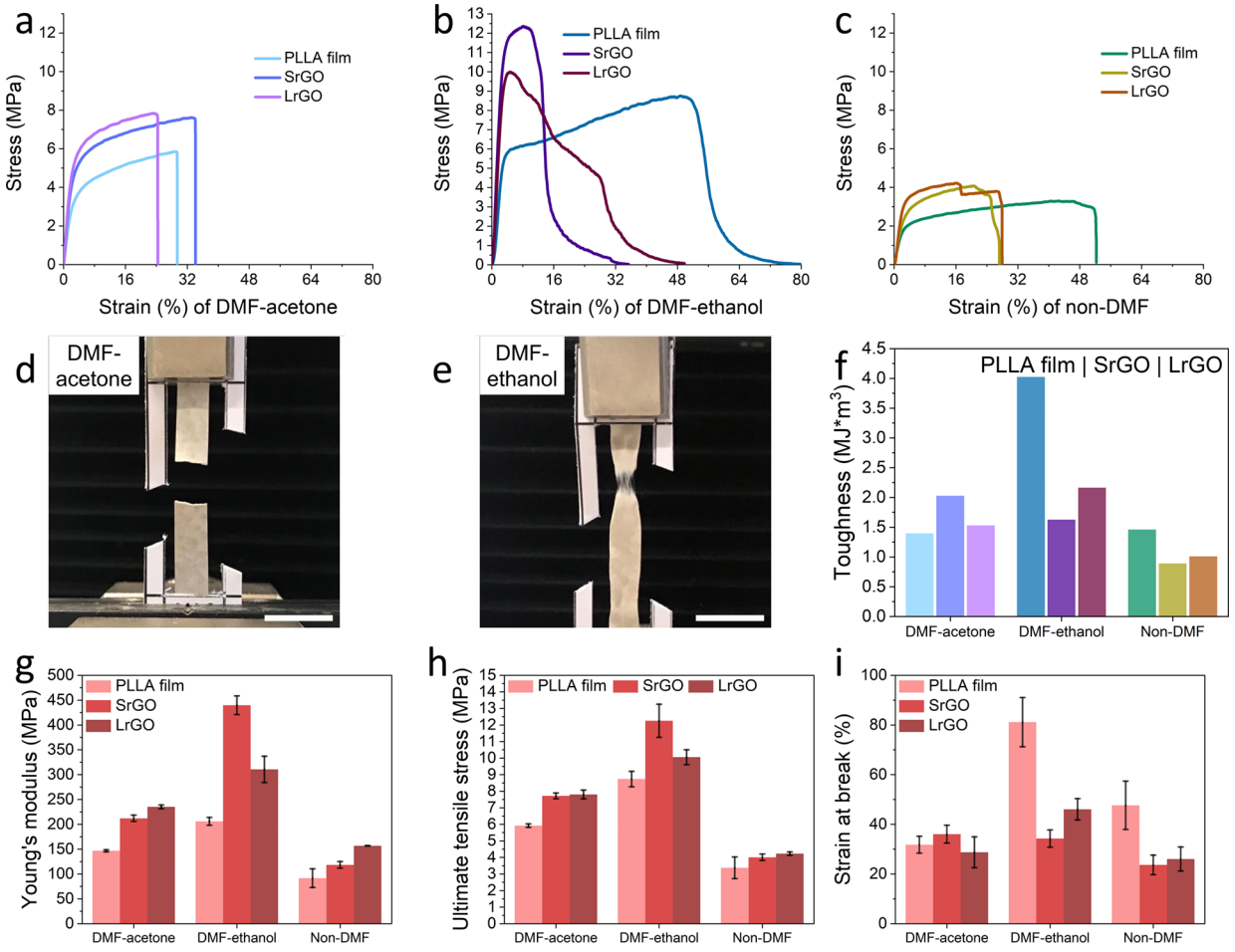

Figure 8. Mechanical performances of three kinds of PLLA/rGO films. (a) Stress−strain curves of the DMF-acetone group PLLA film with rGO coating. (b) Stress−strain curves of the DMF-ethanol group PLLA film with rGO coating. (c) Stress−strain curves of the non-DMF group PLLA film with rGO coating. (d) Optical photo of the DMF-acetone group PLLA film coated with SrGO when it is broken under tensile test. (e) Optical photo of the DMF-ethanol group PLLA film coated with SrGO when it is broken under tensile test. (f) Tensile toughness corresponds to the PLLA film samples displaced in Figure 7a−c. (g) Young's modulus of PLLA films under different treatments and coated with rGO. (h) Ultimate tensile stress of PLLA films under different treatments and coated with rGO. (i) Strains at break of PLLA films under different treatments coated with rGO.

The hydrophilicity and hydrophobicity of GO- and rGO-coated PLLA electrospun films are determined by the flake size of GO and the surface morphology of the PLLA electrospun film. Among the films, the distribution of SGO on the non-DMF film was the most uneven, and the second uneven distribution is that of LGO ultrasonically coated on the DMF-ethanol film. The introduction of a sufficient amount of uniformly distributed GO can effectively improve the hydrophilicity of the PLLA electrospun film. Moreover, the moisture absorption rate of the film with the same surface morphology coated with LGO is higher than that of the one coated with SGO. The reduction of LGO coated on the DMF-ethanol or non-DMF film by LAA aqueous solution could improve the hydrophobicity of the original DMF-ethanol or non-DMF film to some extent, as presented by the optical images in Figure S3. It can be inferred that most of LGO coated on the DMF-acetone film and SGO coated on the DMF-acetone, DMF-ethanol, and non-DMF films by ultrasound were layer-stacking and wrapping the electrospun fibers tightly, so that this kind of GO was difficult to ultimately reduce in a way that was just immersed in LAA aqueous solution. Hence, the hydrophobicity of the DMF-acetone/LrGO, DMF-acetone/SrGO, DMF-ethanol/SrGO, and non-DMF/SrGO films was not effectively improved by the introduction of rGO compared to the pristine PLLA films.

In Figure 7a−c, the XPS spectra of electrospun PLLA fibers dissolved by DCM/DMF dual-solvent with ethanol treatment (DMF-ethanol), GO-coated on DMF-ethanol-electrospun PLLA fibrous films, and rGO-coated on DMF-ethanol-electrospun PLLA fibrous films are presented. For a pure PLLA fiber film sample, four components located at 284.8, 286.6, and 288.8 eV correspond to C−C/C−H, C−O and O−C=O. In Figure 7b,c, it could be observed that C−C presented a higher intensity due to the successful reduction of GO.

In Figure 7d,e, we characterized the morphology of rGO on a silicon wafer and single PLLA nanofibers using AFM. A diluted GO aqueous solution (0.05 mg/mL) was dropped onto the silicon wafers, dried at room temperature, and then reduced in a LAA solution at 80 °C for 24 h. The thickness of rGO on the silicon wafers is approximately 1.2−1.4 nm, indicating that rGO used in this experiment is a few-layered rGO with less than 20 layers. rGO on the silicon wafers exhibits abundant wrinkles and textures, reflecting the true morphology of rGO naturally deposited on the surface.

https://doi.org/10.1021/acsomega.4c01976
ACS Omega 2024, 9, 27358−27368

Furthermore, we conducted an in situ morphology characterization on PLLA-rGO electrospun fibers. Due to the scale limitation of the fibers, a range of 1 × 1 μm was selected for testing. On this fiber surface, there are both larger undulations around 40 nm and smaller undulations around 2−3 nm. We believe that the larger undulations are caused by the porous fiber surface caused by post-treatment, while the smaller and continuous undulations are caused by the coating of rGO on the fiber surface. Because the concentration of rGO solution used for coating the PLLA fiber is much higher than that used for preparing silicon wafer samples, excess rGO is deposited on the fiber surface, resulting in larger undulations on the fiber surface compared with those on the silicon wafer.

3.6. Mechanical Study of PLLA Fibers Coated with GO Nanosheets. Figure 8 presents the tensile mechanical properties of PLLA/rGO fiber films under different parameters. It can be observed that different post-treatments have distinct effects on the film's performance. Comparatively, PLLA fiber films subjected to phase separation through DMF exhibit stronger mechanical properties after post-treatment (DMF-ethanol) compared to pure PLLA fiber (non-DMF), including tensile stress, elongation strain, Young's modulus, and toughness, which is also referred to as fracture energy. On the other hand, the DMF-ethanol group results in better performance than the DMF-acetone group. This may be attributed to the milder and slower nature of ethanol post-treatment, which ensures the crystallinity of the fiber film while avoiding the drastic contraction observed when the fibers are immersed in acetone. Based on these tensile experiments, we found that the acetone post-treatment occurs instantaneously, accompanied by a sharp contraction of the fiber film, sometimes leading to film rupture.

Furthermore, the coating of rGO with different flake sizes also significantly influences the mechanical performance of the PLLA fiber film. The impact of LrGO coating on the fiber performance is slightly weaker than that of SrGO, possibly due to the matching size of SrGO flakes with the mesopore size on the fiber surface. Additionally, vibrations caused by ultrasonication during the coating process may damage PLLA fibers. After rGO coating, the trend reverses for acetone post-treated PLLA fiber films (DMF-acetone), with SrGO exhibiting better performance, surpassing even the fiber film before GO coating. This may be attributed to the larger mesopore diameter achieved through acetone postprocessing, allowing SrGO to embed more into the fiber's pores, leading to enhanced performance.[29]

Considering the practical applications reported for rGO fiber films such as battery cathodes, electromagnetic shielding, and sensors, a continuous and conductive surface graphene coating is essential in these applications. However, the surface of acetone-post-treated PLLA fiber films is excessively rough, making it challenging to form a continuous rGO surface. Therefore, PLLA fiber films processed through DMF phase separation, ethanol post-treatment, and LrGO coating are the preferred choice for potential applications.

4. CONCLUSIONS

Based on the spinning parameter study, the concentrations of PLLA and DMF were determined to fabricate uniform, thin, and smooth fibers. Subsequently, different post-treatments were employed to compare the morphology and structure of the PLLA electrospinning film. Coated with controllable sizes of GO flakes and reduced, PLLA/rGO fibrous films were successfully prepared. Through hydrophilicity and mechanical investigation, it was observed that PLLA fiber films spun from the DCM/DMF solution, post-treated by ethanol, and coated with LrGO are the preferred choice for desired high-strength applications.

■ ASSOCIATED CONTENT

Supporting Information

The Supporting Information is available free of charge at https://pubs.acs.org/doi/10.1021/acsomega.4c01976.

SEM images and size distribution histograms of the graphene oxide flakes; optical photos of PLLA/rGO fibrous films, each photo equivalent to a 4 × 4 cm^2 film; and Raman spectra, XRD patterns, and FT-IR spectra of three groups of PLLA/rGO fibrous films (PDF)

■ AUTHOR INFORMATION

Corresponding Author

Zhongda Chen − *School of Biomedical Engineering and Informatics, Nanjing Medical University, Nanjing 211166, P.R. China;* orcid.org/0000-0003-0518-7938; Email: zhongda.chen@njmu.edu.cn

Authors

Jun Song − *Materdicine Lab, School of Life Sciences, Shanghai University, Shanghai 200444, P.R. China;* orcid.org/0000-0002-7689-1722

Yilu Chen − *Department of Materials, The University of Manchester, Manchester M13 9PL, U.K.*

Complete contact information is available at: https://pubs.acs.org/10.1021/acsomega.4c01976

Notes

The authors declare no competing financial interest.

■ ACKNOWLEDGMENTS

Jun Song was funded by Shanghai Pujiang program (No. 22PJD026) and Suzhou PPM Institute of Functional Materials (No. 2023008). Zhongda Chen was funded by Jiangsu distinguished postdoctoral project (No. 2023ZB469). The authors acknowledge the support of the Electron Microscopy Centre and XRD suite in Department of Materials, The University of Manchester. Jun Song would like to acknowledge Xingyu Pu's spiritual inspiration.

■ REFERENCES

(1) Zeng, W.; Zhao, Y.; Zhang, F.; Li, R.; Tang, M.; Chang, X.; Wang, Y.; Wu, F.; Han, B.; Liu, Z. A general strategy for recycling polyester wastes into carboxylic acids and hydrocarbons. *Nat. Commun.* **2024**, *15* (1), 160.

(2) Smith, D. L.; Vest, N. A.; Convento, M. O.; Montemayor, M. D.; Grunlan, J. C. Buffer induced ionically crosslinked polyelectrolyte treatment for self-extinguishing polyester. *npj Mater. Degrad.* **2024**, *8* (1), 14 DOI: 10.1038/s41529-024-00432-2.

(3) McGuire, T. M.; Buchard, A.; Williams, C. Chemical Recycling of Commercial Poly(l-lactic acid) to l-Lactide Using a High-Performance Sn(II)/Alcohol Catalyst System. *J. Am. Chem. Soc.* **2023**, *145* (36), 19840−19848.

(4) Wang, Z.; Pan, Z. Preparation of hierarchical structured nano-sized/porous poly(lactic acid) composite fibrous membranes for air filtration. *Appl. Surf. Sci.* **2015**, *356*, 1168−1179.

(5) Barton, A. F. M. *CRC Handbook of Solubility Parameters and Other Cohesion Parameters*; 2017.

(6) Natarajan, L.; New, J.; Dasari, A.; Yu, S.; Manan, M. A. Surface morphology of electrospun PLA fibers: mechanisms of pore formation. *RSC Adv.* **2014**, *4* (83), 44082−44088.
(7) Lu, T.; Cui, J.; Qu, Q.; Wang, Y.; Zhang, J.; Xiong, R.; Ma, W.; Huang, C. Multistructured Electrospun Nanofibers for Air Filtration: A Review. *ACS Appl. Mater. Interfaces* **2021**, *13* (20), 23293−23313.
(8) Song, J.; Zhang, B.; Lu, Z.; Xin, Z.; Liu, T.; Wei, W.; Zia, Q.; Pan, K.; Gong, R. H.; Bian, L.; et al. Hierarchical Porous Poly(l-lactic acid) Nanofibrous Membrane for Ultrafine Particulate Aerosol Filtration. *ACS Appl. Mater. Interfaces* **2019**, *11* (49), 46261−46268.
(9) Song, J.; Zhao, Q.; Meng, C.; Meng, J.; Chen, Z.; Li, J. Hierarchical Porous Recycled PET Nanofibers for High-Efficiency Aerosols and Virus Capturing. *ACS Appl. Mater. Interfaces* **2021**, *13* (41), 49380−49389.
(10) Huang, X.; Jiao, T.; Liu, Q.; Zhang, L.; Zhou, J.; Li, B.; Peng, Q. Hierarchical electrospun nanofibers treated by solvent vapor annealing as air filtration mat for high-efficiency PM2.5 capture. *Science China Materials* **2019**, *62* (3), 423−436.
(11) Choi, S. Y.; Cho, I. J.; Lee, Y.; Park, S.; Lee, S. Y. Biocatalytic synthesis of polylactate and its copolymers by engineered microorganisms. *Methods Enzymol.* **2019**, *627*, 125−162.
(12) Li, M.; Chen, X.; Li, X.; Dong, J.; Zhao, X.; Zhang, Q. Controllable Strong and Ultralight Aramid Nanofiber-Based Aerogel Fibers for Thermal Insulation Applications. *Advanced Fiber Materials* **2022**, *4* (5), 1267−1277.
(13) Ke, L.; Yang, T.; Liang, C.; Guan, X.; Li, T.; Jiao, Y.; Tang, D.; Huang, D.; Li, S.; Zhang, S.; et al. Electroactive, Antibacterial, and Biodegradable Poly(lactic acid) Nanofibrous Air Filters for Healthcare. *ACS Appl. Mater. Interfaces* **2023**, *15* (27), 32463−32474.
(14) Bognitzki, M.; Czado, W.; Frese, T.; Schaper, A.; Hellwig, M.; Steinhart, M.; Greiner, A.; Wendorff, J. H. Nanostructured Fibers via Electrospinning. *Adv. Mater.* **2001**, *13* (1), 70−72.
(15) Sekkarapatti Ramasamy, M.; Krishnamoorthi Kaliannagounder, V.; Rahaman, A.; Park, C. H.; Kim, C. S.; Kim, B. Synergistic Effect of Reinforced Multiwalled Carbon Nanotubes and Boron Nitride Nanosheet-Based Hybrid Piezoelectric PLLA Scaffold for Efficient Bone Tissue Regeneration. *ACS Biomater Sci. Eng.* **2022**, *8* (8), 3542−3556.
(16) Xin, G.; Yao, T.; Sun, H.; Scott, S. M.; Shao, D.; Wang, G.; Lian, J. Highly thermally conductive and mechanically strong graphene fibers. *Science* **2015**, *349* (6252), 1083−1087.
(17) Chang, D.; Liu, J.; Fang, B.; Xu, Z.; Li, Z.; Liu, Y.; Brassart, L.; Guo, F.; Gao, W.; Gao, C. Reversible fusion and fission of graphene oxide-based fibers. *Science* **2021**, *372* (6542), 614−617.
(18) Wojasiński, M.; Pilarek, M.; Ciach, T. Comparative Studies of Electrospinning and Solution Blow Spinning Processes for the Production of Nanofibrous Poly(L-Lactic Acid) Materials for Biomedical Engineering. *Polish Journal of Chemical Technology* **2014**, *16* (2), 43−50.
(19) Naga, N.; Yoshida, Y.; Inui, M.; Noguchi, K.; Murase, S. Crystallization of amorphous poly(lactic acid) induced by organic solvents. *J. Appl. Polym. Sci.* **2011**, *119* (4), 2058−2064.
(20) Naga, N.; Yoshida, Y.; Noguchi, K. Crystallization of poly(L-lactic acid)/poly(D-lactic acid) blend induced by organic solvents. *Polym. Bull.* **2019**, *76* (7), 3677−3691.
(21) Feicht, P.; Biskupek, J.; Gorelik, T. E.; Renner, J.; Halbig, C. E.; Maranska, M.; Puchtler, F.; Kaiser, U.; Eigler, S. Brodie's or Hummers' Method: Oxidation Conditions Determine the Structure of Graphene Oxide. *Chemistry* **2019**, *25* (38), 8955−8959.
(22) Beran, A. Infrared Spectroscopy of Micas. *Reviews in Mineralogy and Geochemistry* **2002**, *46* (1), 351−369.
(23) Trivedi, M. K.; Branton, A.; Trivedi, D.; Bairwa, K.; Jana, S. Fourier Transform Infrared and Ultraviolet-Visible Spectroscopic Characterization of Biofield Treated Salicylic Acid and Sparfloxacin. *Nat. Prod. Chem. Res.* **2015**, *3* (5), No. 1000186, DOI: 10.4172/2329-6836.1000186.
(24) Lan, Q.; Yu, J.; He, J.; Maurer, F. H. J.; Zhang, J. Thermal Behavior of Poly(l-lactide) Having Low l-Isomer Content of 94% after Compressed CO2 Treatment. *Macromolecules* **2010**, *43* (20), 8602−8609.
(25) Sami, A.; David, E.; Fréchette, M.;Procedure for evaluating the crystallinity from X-ray diffraction scans of high and low density polyethylene/SiO < inf > 2</inf> composites. In *2010 Annual Report Conference on Electrical Insulation and Dielectic Phenomena*; 2010.
(26) Thakur, S.; Karak, N. Green reduction of graphene oxide by aqueous phytoextracts. *Carbon* **2012**, *50* (14), 5331−5339.
(27) Dresselhaus, M. S.; Jorio, A.; Hofmann, M.; Dresselhaus, G.; Saito, R. Perspectives on carbon nanotubes and graphene Raman spectroscopy. *Nano Lett.* **2010**, *10* (3), 751−758.
(28) Niyogi, S.; Bekyarova, E.; Itkis, M. E.; Zhang, H.; Shepperd, K.; Hicks, J.; Sprinkle, M.; Berger, C.; Lau, C. N.; deHeer, W. A. Spectroscopy of covalently functionalized graphene. *Nano Lett.* **2010**, *10* (10), 4061−4066.
(29) Rocher, L.; Cameron, J.; Barr, J.; Dillon, B.; Lennon, A. B.; Menary, G. H. Linking processing, microstructure and mechanical properties of expanded PLLA tubes for bioresorbable stent applications. *Eur. Polym. J.* **2023**, *195*. 112205.

https://doi.org/10.1021/acsomega.4c01976
ACS Omega 2024, 9, 27358−27368